Probing edge magnetization in antiferromagnetic spin segments

A. Ghirri,[1,2,*] G. Lorusso,[1,2] F. Moro,[1,2] F. Troiani,[1] V. Corradini,[1] C. Muryn,[3] F. Tuna,[3] G. Timco,[3] R. E. P. Winpenny,[3] and M. Affronte[1,2]

[1]*National Research Center on NanoStructures and BioSystems at Surfaces (S3), CNR–INFM, 41100 Modena, Italy*

[2]*Dipartimento di Fisica, Università di Modena e Reggio Emilia, via Campi 213/a, 41100 Modena, Italy*

[3]*The Lewis Magnetism Laboratory, School of Chemistry, The University of Manchester, Oxford Road, Manchester M139PL, United Kingdom*

(Received 18 July 2008; revised manuscript received 29 May 2009; published 25 June 2009)

Antiferromagnetic spin segments are quantum objects with discrete spectrum of excitations. Here we report the characterization of two molecular derivatives, namely, Cr_6InNi and Cr_7InNi, which are odd- and even-membered spin cyclic systems magnetically broken by an In^{3+} ion. Analysis of low-temperature specific heat, susceptibility, and magnetization allows us to determine the microscopic parameters of the spin Hamiltonian and the pattern of the spin excitations. It turns out that the exchange coupling and the anisotropy constants in Cr_6InNi and Cr_7InNi are quite close to those in Cr_7Ni-piv. X-ray absorption experiments evidence that the oxidation state of Cr^{3+} and Ni^{2+} and their local symmetries are essentially the same in the Cr_6InNi, Cr_7InNi, and Cr_7Ni-piv clusters. Thus the main difference resides in the number and topology of spins in the different derivatives. Based on these grounds, we show how the spin of Ni^{2+} can be used as a marker to probe the local magnetization of spin segments by directly comparing the sign and the intensity of the dichroic signal measured in the three derivatives. Quantitative analysis of x-ray absorption spectra allows the evaluation of the spin and orbital magnetic moment in the different derivatives, whose dependence on the magnetic field fits well the results of the microscopic spin-Hamiltonian calculations.

DOI: 10.1103/PhysRevB.79.224430 PACS number(s): 75.50.Xx, 78.70.Dm, 65.40.−b, 75.75.+a

I. INTRODUCTION

Spin waves in infinite chains are textbook examples of excitations in one-dimensional (1D) systems. More recently the interest was turned toward size effects and quantum phenomena in finite systems, namely, magnetic quantum wires or spin segments (finite chains). For instance, the transport of magnetization in a 1D magnetic wire has been theoretically considered for the observation of new phenomena.[1] Propagation of domain walls in magnetic wires has been proposed for elaboration of information by logic magnetic devices,[2] while quantum communication in finite spin chains has been theoretically considered extensively.[3] Such theoretical interest has been recently underpinned by the capability of fabricating 1D magnetic systems with atomistic control. One of the first attempts to create artificial spin segments by aligning atoms on a surface was reported by Gambardella *et al.*[4,5] Good examples of atomic structures were recently engineered by the IBM group:[6] few magnetic Mn atoms were aligned on a CuN surface, thus forming antiferromagnetic spin segments. Molecular chemistry provides alternative routes for fabricating templates and paradigmatic examples of spin segments.[7] The present work provides significant examples of this type.

The finite size of a spin chain leads to a discrete spectrum of excitations. Recently the case of spin waves in molecular spin clusters has been studied in detail: for rings with dominant antiferromagnetic interaction, the low-lying energy spectrum is typically structured in three bands, the lowest one, named L band, is a rotational band that follows the Landé rule $E(S) \propto S(S+1)$.[8–10] These excited states are characterized by the rotation of the oppositely oriented total spins of each sublattice. The second group, named E band, is generated by higher energy excitations, which have analogies with spin waves. The remaining states form a quasicontinuum.[10,11] In Ref. 7 we discussed some consequences of the cyclic symmetry breakings in the spectrum of spin-wave excitations. These works pave the way for searching specific effects or phenomena in these systems. For instance, it is known that edge states in both integer and half-integer chains arise from exchange interactions,[12–16] while localized states[17,18] can be observed when nonlinear effects are significant or specifically induced by extra spins at the edge.[19]

The first aim of this work is to characterize molecular nanomagnets. In particular, we consider heterometallic molecular 1D spin systems comprising mainly Cr^{3+} ions (with spin $s=3/2$) with selected substitutions by Ni^{2+} ($s=1$) and nonmagnetic In^{3+}. Organic ligands (mainly carboxilates) support the dominant antiferromagnetic Heisenberg exchange between nearest-neighboring metal centers. The magnetic properties of these molecules, namely, Cr_6InNi and Cr_7InNi, will be compared with those of the parent Cr_7Ni-piv ring, recently proposed as candidate for the qubit encoding.[20] Since collections of identical and noninteracting molecules can be synthesized in bulk quantity and embedded in crystalline structures, we started using thermodynamic properties (susceptibility, magnetization, and specific heat) to characterize them.

An additional motivation is represented by the identification of local probes, i.e., experimental techniques that may probe the magnetization locally within the spin segment. This will allow, for instance, to test effects at the edges and eventually to read out information in specific positions of the spin segment. Nuclear magnetic resonance, for instance, has been already used to probe the local spin moment distribution in molecular Cr_7Cd rings.[21] Here we exploit the analo-

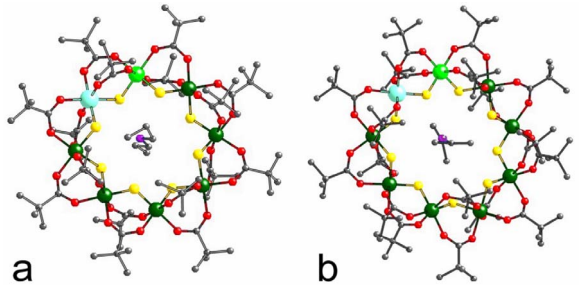

FIG. 1. (Color online) The structures of (a) Cr_6InNi and (b) Cr_7InNi as determined by x-ray diffraction. Colors: Cr—dark green, Ni—light green, In—cyan, F—yellow, O—red, C—black, and N—violet. Hydrogen atoms are omitted for clarity.

gous potentialities of x-ray spectroscopy. In fact, x-ray magnetic circular dichroism (XMCD) was proved to be a powerful tool to study magnetism at molecular level due to its high sensitivity.[22–24] Moreover, thanks to its chemical selectivity, it allows us to separately investigate local symmetries, electronic configuration, orbital, and spin magnetic moments of the magnetic ions.[25–28] The final aim of this work is therefore the following: given similar antiferromagnetic spin segments with ideally only topological differences, we intend to develop protocols to probe the local magnetization.

The paper is organized as follows: synthesis and structural characterization are reported in Sec. II, with further experimental details; Sec. III is devoted to the analysis of specific heat, susceptibility, and magnetization of the derivatives, while Sec. IV reports spectroscopic data and their analysis.

II. EXPERIMENTAL DETAILS

$[H_2NR_2][Cr_6InNiF_8(O_2CCMe_3)_{16}]$ with $R=C_3H_7$, Cr_6InNi in short, was prepared by stirring for 30 min $[(H_2NR_2)_3Cr_6F_{11}(O_2CCMe_3)_{10}]_2$ with $R=C_3H_7$ (1.0 g, 0.27 mmol) (Ref. 29) and $[In_2Ni_2(OH)_2(O_2CCMe_3)_8(HO_2CCMe_3)_2]$ (0.4 g, 0.287 mmol) (Ref. 30) together with pivalic acid (7 g, 68.63 mmol) and diethyl ether (10 ml). Then the solvent was removed by distillation and the residue was heated with constant stirring for 1 h at 150 °C. After cooling to room temperature, acetone (20 ml) was added to the solid and it was stirred for 1 h. The green solid was collected by filtration, washed with acetone, and dried *in vacuo*. $[H_2NR_2][Cr_7InNiF_9(O_2CCMe_3)_{18}]$ with $R=isC_3H_7$, Cr_7InNi in short, was obtained similarly to Cr_6InNi by using $[H_2NR_2][Cr_7InNiF_9(O_2CCMe_3)_{18}]$ with $R=isC_3H_7$. Full details of the synthesis are reported elsewhere.[31]

Crystallographic structures of Cr_6InNi and Cr_7InNi are shown in Fig. 1.[32] Metals are placed at the vertex of regular octagon and nonagon, having a side length of 3.4 Å. Their chemical bridging occurs by means of one fluoride bridge and two 1,3-bridging pivalates either for Cr_6InNi or for Cr_7InNi. The local symmetry of each chromium, indium, or nickel is represented by an octahedron with six apical atoms: four O and two F atoms, equidistant from the metal ion (1.97 ± 0.03 Å), which lies in a slightly distorted octahedral (O_h) environment. Due to the incomplete equivalence between F and O, the symmetry of the coordination around each ion is formally C_2. However, the very similar bond lengths and angles around the magnetic ion leads to an almost perfect equivalence between F and O, which allow the assumption of a nearly pure O_h symmetry even for what concern the charge and spin densities as evidenced by density-functional theory calculations.[33] The similarity in the metal-F-metal and O-C-O angles, which, respectively, range between 124°–126° and 120°–123° for Cr_6InNi and between 124°–130° and 118°–123° for Cr_7InNi, indicates comparable nearest-neighbor exchange coupling in both clusters. Due to the synthetic procedure that we have followed which introduces Ni^{2+} and In^{3+} in the same starting compound, their positions will be one after the other in the final cyclic structure and this implies that $s(Ni^{2+})=1$ is at the edge of the spin segment. This is consistent with crystallographic refinements.

Measurements of thermodynamic properties were performed on microcrystalline powders. Magnetization and susceptibility experiments were carried out by means of a superconducting quantum interference device magnetometer (Quantum Design MPMS-7T). Susceptibility data were collected applying a fixed field of 0.1 T. Heat capacity was measured in the temperature range of 0.3–20 K by means of a Quantum Design PPMS-7T system and ^{3}He refrigerator, using the relaxation method and two-tau fitting. Microcrystalline samples were pressed in thin pellets having a mass of about 2 mg.

X-ray absorption spectroscopy (XAS)-XMCD experiments were performed at the ID8 beamline of the European Synchrotron Radiation Facility (ESRF) in Grenoble (France) using a cryogenic setup that allows the cooling of the specimen down to 10 K at the base pressure of 1.0×10^{-10} mbar. External magnetic field up to $H=\pm5$ T is supplied by means of a superconducting coil. We employed an Apple II undulator that provides high flux (10^{13} photons/s) of polarized light. In order to avoid sample damaging by radiation exposure, measurements were conducted attenuating the beam flux by more than one order of magnitude. Integrity checks with XAS spectra were effectuated throughout the experiment, without finding any trace of degradation. Spectroscopic data were acquired investigating thick films of Cr_6InNi and Cr_7InNi clusters, obtained by drop casting a saturated solution in dichloromethane on graphite substrates. The thickness of the film was sufficiently high to prevent the emission from the substrate. XAS-XMCD spectra were taken at the Cr and Ni $L_{2,3}$ edges in total yield mode with circularly polarized light and $\simeq100\%$ polarization rate. The experimental geometry has the incident beam pointing perpendicular to the surface of the sample and parallel to the direction of the applied magnetic field (**H**). The XMCD spectrum is calculated from the difference between two XAS spectra taken with opposite photon helicity, antiparallel ($\sigma^{\uparrow\downarrow}$) or parallel ($\sigma^{\uparrow\uparrow}$) to the magnetization of the sample (**M**). In order to minimize field inhomogeneities, absorption spectra are evaluated considering the mean value of two opposite directions of **M**, obtained for each polarization, reversing the direction of the applied field **H**.

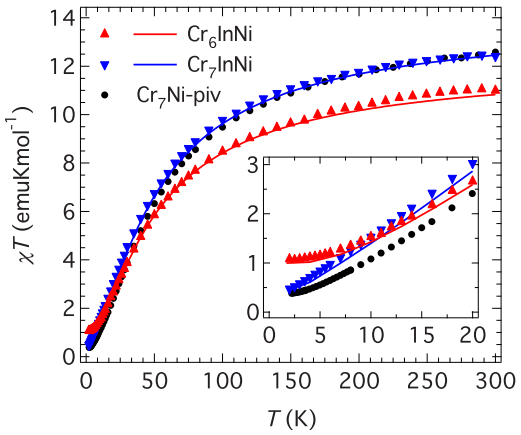

FIG. 2. (Color online) Molar susceptibility plotted as χT vs T for Cr_6InNi, Cr_7InNi, and Cr_7Ni-piv polycrystalline samples. The measurements are performed by applying a static field of 0.1 T. Solid lines represent the curves calculated within spin-Hamiltonian approach as described in the text. (Inset) Magnification at low temperature.

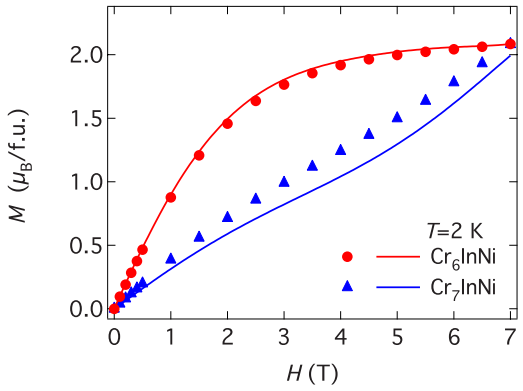

FIG. 3. (Color online) The magnetic field dependence of the magnetization $M(H)$ measured at fixed temperatures on Cr_6InNi and Cr_7InNi polycrystalline samples. Solid lines represent the calculated curves.

III. THERMODYNAMIC PROPERTIES

The Cr_6InNi and Cr_7InNi molecules are first characterized by thermodynamic measurements. The measured quantities are compared with the simulated ones, obtained within a spin-Hamiltonian model.[34] The specific spin Hamiltonian that has already reproduced the magnetic behavior of parent compounds reads

$$\mathcal{H} = \sum_{i=1}^{N-1} J_i \mathbf{s}_i \cdot \mathbf{s}_{i+1} + \sum_{i=1}^{N} d_i [s_{z,i}^2 - s_i(s_i+1)/3] + \mu_B \sum_{i=1}^{N} g_i \mathbf{H} \cdot \mathbf{s}_i \tag{1}$$

with N as the number of magnetic ions. Here, the first term accounts for the dominant exchange interaction between nearest-neighboring ions ($\mathcal{H}_{ex}$); the second and third terms describe the interaction with the local (axial) crystal field ($\mathcal{H}_{cf}$) and the Zeeman coupling ($\mathcal{H}_Z$) to applied magnetic field, respectively. The eigenvalues are obtained by directly diagonalizing the dominant part of the Hamiltonian, namely, $\mathcal{H}_0 \equiv \mathcal{H}_{ex} + \mu_B g_{Cr}\ \mathbf{H}\cdot\mathbf{S}$. The effect of the additional terms ($\mathcal{H}_1$) are included within first-order perturbation theory, being $\mathcal{H}_1 = \mathcal{H}_{cf} + (g_{Ni} - g_{Cr})\ \mathbf{H}\cdot\mathbf{s}_N$. Being the two molecular systems here considered closely related to the unbroken Cr_7Ni-piv rings, we adopt for the physical parameters that enter in the spin Hamiltonian the same values: $J_{Cr\text{-}Cr}/k_B = 17.0$ K, $J_{Cr\text{-}Ni}/k_B = 19.6$ K, $d_{Cr}/k_B = -0.36$ K, $d_{Ni}/k_B = -7$ K, $g_{Cr} = 1.98$, and $g_{Ni} = 2.2$.[35] The presence of a nonmagnetic ion In^{3+}, however, modifies from the magnetic point of view the topology of the molecule, making it an open, rather than a cyclic structure.

In Fig. 2 the temperature (T) dependence of the molar susceptibility χ is plotted as χT vs T for both the Cr_6InNi and Cr_7InNi compounds. For comparison the χT vs T curve of Cr_7Ni-piv is also plotted in this figure. In the temperature range of 20–300 K the three derivatives display a similar behavior. At room temperature the χT values are close to those expected for uncoupled paramagnetic ions: $\chi T(300\ \text{K}) = 12.5$ emu K mol^{-1} for Cr_7Ni-piv and Cr_7InNi and $\chi T(300\ \text{K}) = 11.4$ emu K mol^{-1} for Cr_6InNi. Below 10 K the χT vs T curves of Cr_6InNi and Cr_7InNi have a different behavior (see inset of Fig. 2): for the former χT saturates at 1.1 emu K mol^{-1}, suggesting a ground state with total spin $S=1$. Conversely, for the latter, χT progressively decreases getting close to the value attained for Cr_7Ni-piv at 2 K. This suggests ground-state spin $S=1/2$ with excited states closely spaced in energy for Cr_7InNi.

Figure 3 shows the magnetization (M) as a function of the applied magnetic field (H) for Cr_6InNi and Cr_7InNi. At 2 K, a different behavior for the two derivatives is well visible: for Cr_6InNi, the $M(H)$ curve is close to a simple Brillouin function saturating at about $2.1\mu_B$, whereas for Cr_7InNi the $M(H)$ curve shows a continuous increase with the field H. In agreement with the susceptibility data, this behavior indicates different spins and energy separations of the low-lying magnetic states of the two molecules.

The temperature dependence of the specific heat (C) taken at fixed values of H is plotted in Fig. 4 for Cr_6InNi [panel (a)] and for Cr_7InNi [panel (b)]. At high temperature the lattice contribution dominates, while for $T<7$ K, features of the magnetic contribution become clearly visible. For Cr_6InNi, the latter indeed displays two distinct Schottky anomalies in zero field: a first one in the few K range is related to the energy gap $\Delta_{ex} \simeq 15$ K between the ground and the lowest-lying excited multiplets and a second one, peaked below 1 K, evidences the zero-field splitting of the ground state ($\Delta_{zfs} \simeq 1$ K). For Cr_7InNi, the Schottky anomaly due to the intermultiplet separation (Δ_{ex}) is found with a broad maximum at low temperatures ($\simeq 3$ K), thus confirming that the energy spacing between the lowest multiplets is smaller than in Cr_6InNi and in agreement with the susceptibility and magnetization data.

More quantitative information can be obtained by diagonalizing spin Hamiltonian (1). The specific heat comprises both magnetic and lattice-related contributions, $C = C_{mag} + C_{latt}$.[36] Concerning the latter, below 20 K it is mainly due to the acoustic branches of phonons and it can be fitted by the phenomenological (Debye-like) expression

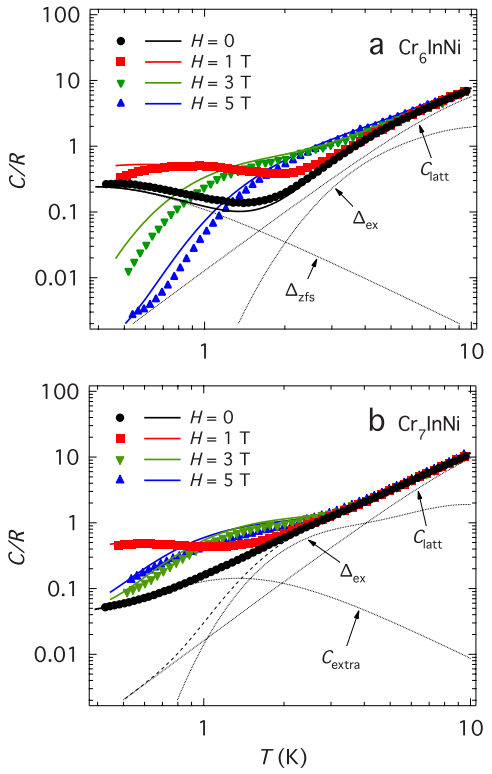

FIG. 4. (Color online) Specific heat $C(H,T)$ normalized to the gas constant R, measured on (a) Cr_6InNi and (b) Cr_7InNi. Solid lines represent the numerical simulations.

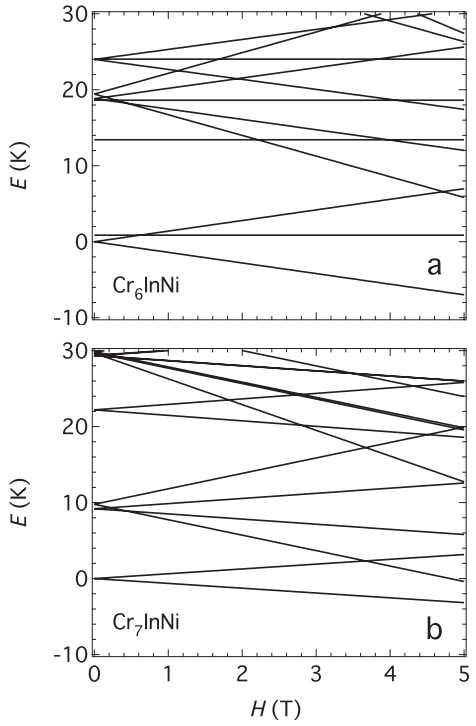

FIG. 5. Low-lying energy levels of (a) Cr_6InNi and (b) Cr_7InNi as a function of the magnetic field applied along the axis perpendicular to the ring. Energy levels are calculated by diagonalizing Eq. (1) with the parameters reported in the text.

$$\frac{C_{\text{latt}}}{R} = \frac{234rT^3}{(\Theta_D + \delta T^2)^3}, \tag{2}$$

as discussed in Ref. 37. For the specific-heat plots (Fig. 4), C_{latt} has been estimated by using Eq. (2) together with $r=295$, $\Theta_D=175$ K, and $\delta=0.55$ K^{-1} for Cr_6InNi and $r=329$, $\Theta_D=168$ K, and $\delta=0.32$ K^{-1} for Cr_7InNi. The magnetic contribution C_{mag} can be written as[36]

$$\frac{C_{\text{mag}}}{R\beta^2} = \frac{\sum_j \epsilon_j^2 e^{-\beta\epsilon_j} \sum_j e^{-\beta\epsilon_j} - \left[\sum_j \epsilon_j e^{-\beta\epsilon_j}\right]^2}{\left[\sum_j e^{-\beta\epsilon_j}\right]^2} \tag{3}$$

with $R=8.314$ J mol^{-1} K^{-1} being the gas constant.

The theoretical simulation is obtained by plugging in the above expression the eigenvalues of the Hamiltonian in Eq. (1) and by averaging on the relative orientation of magnetic field and easy axis direction in order to reproduce the random orientation of the molecules in the powder sample. The agreement with the experimental data is remarkably good even by using for both Cr_6InNi and Cr_7InNi the same values of the exchange and the anisotropy constants reported in Ref. 35 for Cr_7Ni-piv (see above). This clearly demonstrates the capability of selectively introducing local changes in the chemical composition and topology of a given molecule, without altering the remaining interactions within the molecule. We checked that little changes (<10%) of the microscopic parameters may better fit single set of experimental data but for the level of discussion we intend to pursue here that we did not refine the fitting values. We anticipate that the same set of parameters will be also used to interpret the local magnetization extracted by XMCD experiments (Fig. 9) and this is also intentionally done in order to better evidence topology effects in the spin cyclic systems under investigation.

The resulting patterns of the lowest-lying energy levels are plotted in Fig. 5 as a function of the magnetic field. For Cr_6InNi the ground state ($S=1$) is separated by an energy gap of 13.4 K from the first excited state ($S=0$). The overlying multiplets are found with barycenter at 19.0 K ($S=2$) and 24.0 K ($S=1$). For Cr_7InNi, the energy gaps between the ground state ($S=1/2$) and the barycenters of the first excited ($S=3/2$) and second-excited ($S=1/2$) multiplets are at 9.5 and 22.2 K, respectively.

The specific-heat curves at $H=0$ and 1 T of Cr_7InNi are reproduced by adding an extra background C_{extra} at temperatures below few K. With reference to panel (b), the measured C/R (markers) is found close to 0.1 at 1 K while the model calculations (dashes) display a progressive decrease in $C(H=0)$ vs T for $T<2$ K, as expected for the ground doublet. We note, however, that the maximum of C_{extra} is only $C/R \approx 0.1$ at 1 K, which is almost one order of magnitude smaller than what expected for any Schottky anomaly involving the whole sample. Therefore we are led to conclude that this background anomaly of the C vs T curves is due to a small fraction (few percent) of impurity (damaged rings, isolated monomers, etc.) in this sample.

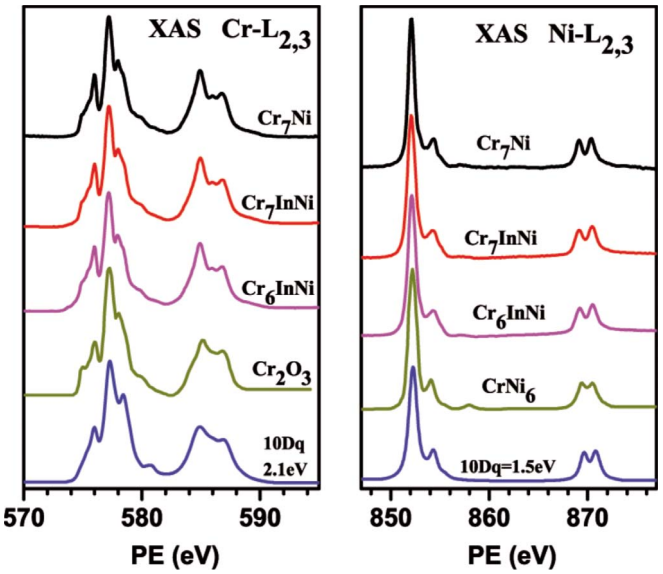

FIG. 6. (Color online) Left panel: Cr $L_{2,3}$ XAS spectra taken for Cr_7Ni, Cr_7InNi, and Cr_6InNi at $T=10$ K and $H=5$ T compared with α-Cr_2O_3 (Ref. 42) and calculations in D_{4h} symmetry ($10Dq=2.1$ eV, $Ds=0.05$ eV). Right panel: Ni $L_{2,3}$ XAS spectra compared with $CrNi_6$ (Ref. 26) and calculations in O_h symmetry ($10Dq=1.5$ eV, $Ds=0$).

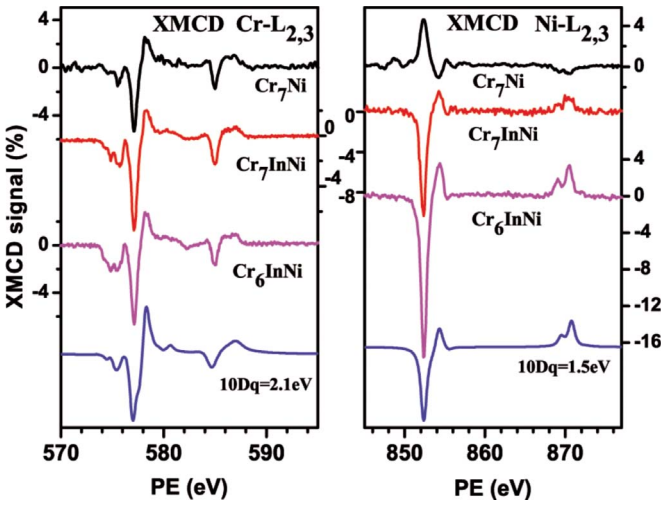

FIG. 7. (Color online) XMCD spectra taken for Cr_7Ni, Cr_7InNi, and Cr_6InNi at the Cr $L_{2,3}$ (left) and Ni $L_{2,3}$ (right) edges at $T=10$ K and $H=5$ T, compared with calculations for Cr^{3+} in D_{4h} symmetry ($10Dq=2.1$ eV, $Ds=0.05$ eV) and for Ni^{2+} in O_h ($10Dq=1.5$ eV, $Ds=0$).

IV. SPECTROSCOPIC RESULTS

We have investigated thick films of Cr_6InNi and Cr_7InNi by means of XAS and XMCD and compared the results with those obtained for a similar sample of Cr_7Ni-piv closed ring.[28] In a submonolayer distribution of functionalized clusters, the interactions with the surface may play a crucial role[23,38–40] and results need to be analyzed with particular care.[41] Here we are interested in directly comparing the magnetic behavior of closed and open rings. For this reason, pristine-nonfunctionalized molecules were simply diluted in solution and deposited on substrates forming thick films.

A. XAS

We first checked the chemical integrity of the deposited molecules by x-ray absorption. The XAS spectrum provides information concerning both the oxidation states and the local symmetries of each transition-metal element. As discussed in the experimental section, the chemical/crystallographic environment of each Cr^{3+} and Ni^{2+} ion is very similar in all the Cr_6InNi, Cr_7InNi, and Cr_7Ni-piv derivatives,[28] with a slightly distorted octahedral symmetry for all the metal sites. In Fig. 6, left panel, the Cr $L_{2,3}$ XAS spectra taken for the Cr_6InNi, Cr_7InNi, and Cr_7Ni-piv rings are compared with that of the α-Cr_2O_3 (Cr^{3+} oxidation state and C_3 slightly distorted O_h symmetry[42,43]). All the Cr absorption spectra present the same profile as in the case of α-Cr_2O_3. In the spectral line shape eight similar features can be identified, which are the direct fingerprint of the presence of Cr^{3+} in an octahedral environment.[42,43] In Fig. 6, right panel, the Ni $L_{2,3}$ XAS spectra for the Cr_6InNi, Cr_7InNi, and Cr_7Ni-piv rings are compared with that of the $CrNi_6$ cluster (Ni^{2+} oxidation state and slightly distorted O_h symmetry[26]). All the Ni absorption spectra present the same line shape of the $CrNi_6$ system, showing unambiguously the presence of a high-spin Ni^{2+} ion in octahedral environment.[26]

Simulation of XAS spectra

We have calculated the $L_{2,3}$ edges absorption for the Ni^{2+} and Cr^{3+} using the ligand-field multiplet model implemented by Thole.[44,45] The calculation takes into account spin-orbit coupling and treats the environment of the absorbing atom through the crystal-field parameters ($10Dq$, Ds, and Dt). The transitions involved in the atomic calculations are $2p^63d^8 \rightarrow 2p^53d^9$ and $2p^63d^3 \rightarrow 2p^53d^4$ for the Ni^{2+} and Cr^{3+}, respectively. In the present paper, the hybridization effects were included by reducing the Slater integrals to 80% and no charge-transfer multiplet calculations were performed. In O_h symmetry the $3d$ orbitals are split into e_g and t_{2g} orbitals with an energy difference of $10Dq$. A further lowering of the symmetry to D_{4h} splits the orbitals by the additional Ds and Dt parameters. The ligand field parameters were tuned to fit the XMCD and isotropic XAS experimental spectra. For the Ni^{2+} the best fit was obtained by considering an O_h symmetry with $10Dq=1.5$ eV and $Ds=Dt=0$, whereas for Cr^{3+} we found a slightly distorted D_{4h} symmetry ($10Dq=2.1$ eV, $Ds=0.05$ eV, and $Dt=0$). This small Ds value also allows us to consider as octahedral the symmetry of the Cr^{3+} ions. The calculated spectra at the $L_{2,3}$ edges, shown in Figs. 6 and 7, are broadened with a Lorentzian ($W_{L_3}=0.2$ and 0.4 eV and $W_{L_2}=0.6$ and 0.4 eV for Cr^{3+} and Ni^{2+}, respectively) and Gaussian ($W_G=150$ meV) to simulate the core hole lifetime and the experimental resolution. The magnetic field is accounted by the Zeeman term in the Hamiltonian. The random orientation of the molecules in such drop-cast samples would require us to perform angular averages of the absorption cross section for all possible orientations of the magnetic

field with respect to the molecular axes. However, van Elp and Searle[46] found that, at least in case of Ni^{2+} and Cr^{3+} in O_h symmetry, the differences between the XAS spectra taken at different orientations were vanishingly small. Therefore, in Figs. 6 and 7 we only report the case where the magnetic field is oriented along the [001] crystallographic axis. In summary, the absorption spectra of the three derivatives are well simulated by the same set of fit parameters indicating the equivalence of oxidation states and chemical environment for the Cr^{3+} and Ni^{2+} ions.

B. XMCD

Figure 7 shows the XMCD spectra taken at 10 K and 5 T for Cr_7Ni-piv, Cr_6InNi, and Cr_7InNi. The line shape of the dichroic signals, although not the intensities, is comparable among the different systems. It is well known that the intensity of the dichroic signal provides information on the local magnetic moments while the sign carries information on the nature of the exchange interactions.[25,47] The intensities of the Cr $L_{2,3}$ dichroic signals are comparable for the three specimens and the sign is the same (Fig. 7). In particular, the negative signal at the Cr L_3 edge and the positive one at the L_2 edge show that, in the range of temperature and field that we have considered, the total Cr magnetic moment points parallel to **H** in each system. Conversely, the dichroic signal taken at the Ni $L_{2,3}$ edges changes significantly (intensity and sign) from case to case. For magnetically broken Cr_6InNi and Cr_7InNi rings, a negative XMCD peak at the L_3 edge and a positive one at the L_2 edge show that the Ni^{2+} magnetic moment is parallel to **H**. On the contrary, for cyclic Cr_7Ni-piv rings the magnetic moment of Ni lies antiparallel to **H**.[28]

Interpretation is not straightforward since the magnetization of a specific site is determined by the state of the whole spin segment and at 10 K different low-lying states are significantly populated (see Fig. 5). Yet, the sign of Ni spin is determined by a competition between the Heisenberg antiferromagnetic coupling with the neighbor spins and the Zeeman interaction. In Cr_7Ni-piv closed ring, spins are arranged in a staggered configuration and the magnetization at the Ni site turns out to be opposite to the average magnetization at Cr sites at 10 K.[28] Due to the presence of In^{3+}, which breaks the Heisenberg exchange coupling, we expect that the behavior of the magnetic moment of nickel is dominated by the Zeeman term in both Cr_6InNi and Cr_7InNi, and the sign of magnetization at the Ni site turns out to be the same as the total magnetization of Cr, i.e., parallel to the applied magnetic field. This fact qualitatively proves that Ni is sensitive to the spin arrangement along the ring or segment.

XMCD calculations

Quantitative information on the Cr^{3+} and Ni^{2+} spin and orbital magnetic moments can be obtained by using the XMCD sum rules.[48,49] In the literature, the applicability of such rules is a controversial argument because of arbitrary assumptions, concerning the number of 3*d* holes, the dipolar term $\langle T_z \rangle$, and the *j*-*j* mixing effect that must be taken into account. In Ref. 28 we have already discussed the validity of sum rules calculations for Cr_7Ni-piv; in the following we discuss their applicability to Cr_6InNi and Cr_7InNi.

Since each Cr^{3+} and Ni^{2+} ion in Cr_7InNi and Cr_6InNi is in a slightly distorted O_h symmetry, the t_{2g} and e_g manifolds possess a nearly isotropic charge density, thus causing the quadrupole charge density term to vanish. Thus for the number of 3*d* holes we have directly used the nominal values of $N_{\mathrm{eff}}=7$ for Cr^{3+} and $N_{\mathrm{eff}}=2$ for Ni^{2+} neglecting the anisotropic terms. For the general case of 3*d* metal the $\langle T_z \rangle$ is expected to be finite. Nevertheless, in our particular case of $3d^3$ (Cr^{3+}) and $3d^8$ (Ni^{2+}) ions in O_h symmetry the $\langle T_z \rangle$ term is negligible,[50,51] allowing the application of the isotropic sum rules.[52]

For the calculations it is useful to define three parameters: $r=I_{L_3}+I_{L_2}$ is the integral of the whole absorption spectrum obtained from the sum of $\sigma^{\uparrow\uparrow}$ and $\sigma^{\uparrow\downarrow}$ and $p=A$ and $q=A+B$ can be directly derived from the intensity of the dichroic signal at the $L_3(A)$ and $L_2(B)$ edges (Fig. 8). The orbital (m_o) and spin (m_s) magnetic moments can be evaluated with the following expressions:[53]

$$\frac{m_o}{\mu_{\mathrm{B}}} = -\frac{4q}{3r} N_{\mathrm{eff}} \tag{4}$$

and

$$\frac{m_s}{\mu_{\mathrm{B}}} = -\frac{(6p-4q)}{r} N_{\mathrm{eff}}. \tag{5}$$

When the spectral features of the L_2 and L_3 edges overlap, the absorption process involves a quantum superposition of $2p_{3/2}$ and $2p_{1/2}$ excitations, which reduces the spin moment. This overlap is negligible for the heavy transition metals, due to their large $L_{2,3}$ spin-orbit splitting. In the case of Ni the application of the sum rules is straightforward whereas the case of Cr is controversial in the literature. Indeed, for light transition metals, such as Cr, the 2*p* spin-orbit splitting is small, the *j*-*j* mixing is strong, and the sum rule underestimates the value of the spin magnetic moment. This discrepancy has been theoretically quantified for $3d^n$ systems by Crocombette *et al.*[51] and Teramura *et al.*[54] Thus, in a simplified approach, one can get a rough estimation of the magnetic moment multiplying the spin moment sum rule by a spin correction (SC) factor.[51,54,55] We have already used a SC=1.75 for the Cr_8 and Cr_7Ni-piv rings and verified its validity comparing the results with standard magnetization measurements.[28] Since the shape of the Cr $L_{2,3}$ absorption spectra is exactly the same, for Cr_6InNi and Cr_7InNi we use the same SC value of 1.75 ± 0.05. As it will be discussed in the following, the comparison with spin-Hamiltonian calculations and bulk magnetization measurements confirms the effectiveness of this choice. This value is in excellent agreement with atomic calculations that take into account the multipole electron-electron interaction.[54] For a $3d^4$ ion in O_h symmetry with $10Dq=1.5$ eV (which are almost the same conditions of the Cr^{3+} ions in our systems) these calculations predict a correction factor of 1.70.

Equation (4) points out that m_o is proportional to q, thus the vanishing of the dichroic signal integral at the Cr $L_{2,3}$ edges ($q=0$) shows the complete quenching of the orbital

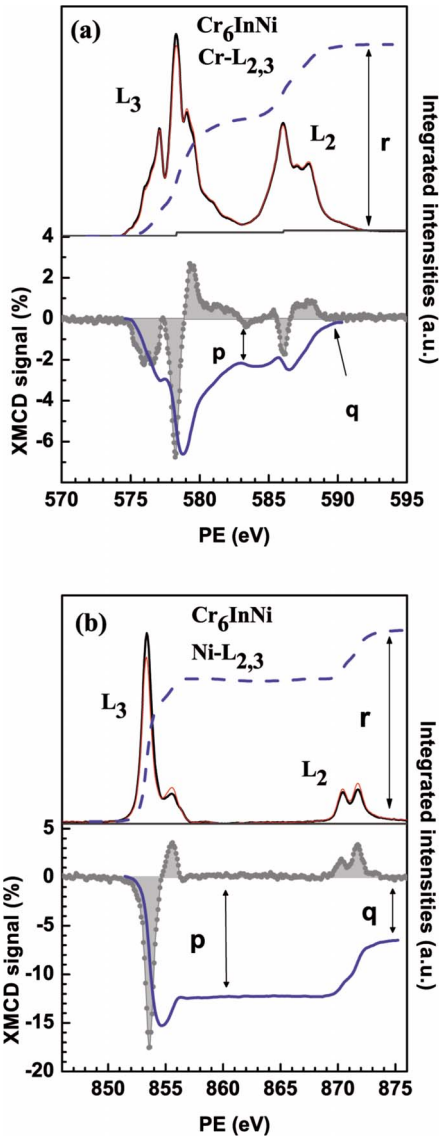

FIG. 8. (Color online) Upper panels: (a) Cr and (b) Ni $L_{2,3}$ XAS spectra taken with $\sigma^{\uparrow\uparrow}$ and $\sigma^{\uparrow\downarrow}$ circularly polarized lights and the XAS integral (dashed line) at 5 T and 10 K for Cr_6InNi. Lower panels: XMCD spectra (dotted lines) and their integrals (continuous lines). The p, q, and r values are calculated upon the removal of the L_3 and L_2 edge jumps by subtracting a two-steplike function from the absorption spectrum.

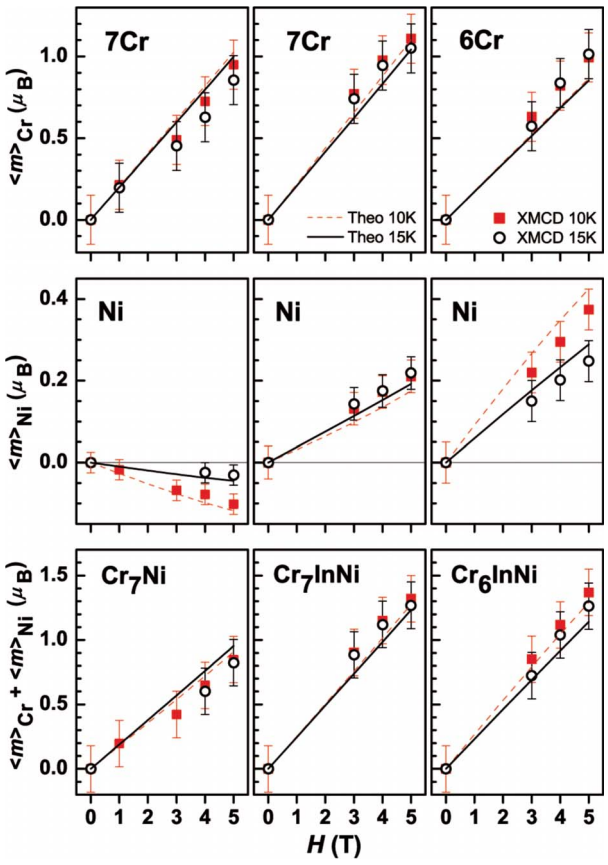

FIG. 9. (Color online) Magnetic moment vs field curves derived by XMCD sum rules. Data measured on the same derivative are arranged in columns, where the horizontal panels show, respectively, the partial contribution of chromium, nickel, and their sum. The uncertainty of the magnetic moment takes into account the signal-to-noise ratio of the related spectrum. Solid lines represent the spin-Hamiltonian calculations. Both XMCD data and calculations shown for Cr_7Ni-piv (left panels) are taken from Ref. 28.

momentum of Cr^{3+} due to the crystal field, so it follows that $g_{Cr}=2.0\pm0.1$. For Ni^{2+}, conversely, the value of $q\neq0$ indicates the partial quenching of the orbital momentum. The sum rules show that in every system $m_o(\mathrm{Ni})/m_s(\mathrm{Ni})\approx10\%$; thus we can estimate the gyromagnetic factor to be $g_{Ni}=2.2\pm0.1$. The so obtained gyromagnetic factors are in good agreement with those that fit the thermodynamic measurements (see above).

By means of Eqs. (4) and (5) we have evaluated the mean value of the spin and orbital magnetic moments $\langle m\rangle=\langle m_o+m_s\rangle$ and in Fig. 9 we show its dependence on the magnetic field for $T=10$ and 15 K. For Cr^{3+} the data derived from the dichroic signal reflect the mean value of the magnetic moments over the six or seven sites of the segment, so in the upper panels we have estimated $\langle m\rangle_{Cr}$ by multiplying the mean value for the number of Cr sites. As expected the curves look similar for the three derivatives because the local information is washed out. Conversely, $\langle m\rangle_{Ni}$ is calculated from the dichroic signal of Ni^{2+} and the plot of $\langle m\rangle_{Ni}$ vs H shows remarkable differences from one cluster to another (central panels). According in Fig. 7, the magnetic moment of Ni has negative slope in cyclic Cr_7Ni-piv rings and positive slope in magnetically Cr_6InNi and Cr_7InNi rings. Furthermore, the higher magnitude for Cr_6InNi with respect to Cr_7InNi at 10 K shows how the magnetic moment of Ni is sensitive to the topology of the spin segment.

A quantitative description of the experimental behaviors reported in Fig. 9 can be derived from the spin-Hamiltonian calculations. The measured magnetic moments are, in fact, compared with their theoretical counterparts, namely, $\langle m\rangle_{Cr}=\mu_B g_{Cr}\Sigma_{i=1}^{N-1}\langle s_{z,i}\rangle$ and $\langle m\rangle_{Ni}=\mu_B g_{Ni}\langle s_{z,N}\rangle$. At the temperature of 10 and 15 K several magnetic states are already thermally populated and contributed to the magnetization (Fig. 5). The above averages thus result from the statistical contributions from ~100 eigenstates, weighted by the Boltzmann factors. The calculated curves, obtained without applying any fitting

procedure, are displayed as solid lines in Fig. 9. The good agreement between theoretical and experimental curves confirms the validity of the magnetic moments $\langle m\rangle_{Cr}$ and $\langle m\rangle_{Ni}$ derived by the XMCD sum rules. The lower panels display the total magnetization of the cluster estimated as $\langle m\rangle_{Cr}+\langle m\rangle_{Ni}$ from sum rules. The dependence on the magnetic field shows agreement with both the calculated curve and the bulk magnetization (not shown) at 10 and 15 K.

V. CONCLUDING REMARKS

We succeeded in synthesizing two molecular derivatives, namely, Cr_6InNi and Cr_7InNi, which are good examples of even- and odd-membered antiferromagnetic spin segments with a Ni^{2+} spin at one edge. By means of magnetometry and calorimetry we have characterized the magnetic features of these systems. We then exploited XMCD spectroscopy to investigate the local magnetization of the Cr^{3+} and Ni^{2+} ions and we compared these results with those obtained on Cr_7Ni-piv molecular rings. We show that the dichroic signal taken at the Ni $L_{2,3}$ edges is particularly sensitive to the topology or nuclearity of the cyclic system, evidencing that, in magnetically broken rings, the spin of nickel tends to be aligned along the magnetic-field direction. Simulations performed within a spin-Hamiltonian model and using the same microscopic parameters estimated for the Cr_7Ni-piv closed ring are in good agreement with all the above measurements. This clearly demonstrates the capability of introducing selective changes in the spin-chain topology or nuclearity without affecting the remaining interactions.

In order to fully exploit the potentialities of XMCD as a tool for locally probing molecular magnets, a higher degree of selectivity has to be achieved. This goal will be pursued mainly in two directions. First, by performing XMCD experiments at lower temperatures ($\sim$1 K) in order to avoid statistical average over a large number of quantum states, which washes out part of the specific features possessed by these molecular systems. Second, the addition of further selective chemical substitutions in the spin segment might allow to individually address more than one spin within the chain.

ACKNOWLEDGMENTS

This work has been carried out within the framework of the EU Network of Excellence "MAGMANet" (Contract No. 515767) and supported by FP7-ICT FET Open "MolSpinQIP" project (Contract No. 211284), by Italian Ministry of Research (PRIN No. 2006029518), and by EPSRC (UK). We acknowledge ESRF for provision of synchrotron-radiation facilities. It is a pleasure to thank F. Borsa, A. Lascialfari, S. Carretta, P. Santini, and G. Amoretti for stimulating discussions and J. Criginsky Cezar, M. Evangelisti, A. Candini, and T. D. Nguyen for assistance during the experiments.

*Corresponding author; alberto.ghirri@unimore.it

[1] F. Meier and D. Loss, Phys. Rev. Lett. **90**, 167204 (2003).
[2] D. A. Allwood, G. Xiong, C. C. Faulkener, A. Atkinson, D. Petit, and R. P. Cowburn, Science **309**, 1688 (2005).
[3] S. Bose, B.-Q. Jin, and V. E. Korepin, Phys. Rev. A **72**, 022345 (2005); S. Bose, Contemp. Phys. **48**, 13 (2007), and references therein.
[4] P. Gambardella, A. Dallmeyer, K. Maiti, M. C. Malagoli, W. Eberhardt, K. Kern, and C. Carbone, Nature (London) **416**, 301 (2002).
[5] P. Gambardella, Nature Mater. **5**, 431 (2006).
[6] C. F. Hirjibehedin, C. P. Lutz, and A. J. Heinrich, Science **312**, 1021 (2006).
[7] A. Ghirri, A. Candini, M. Evangelisti, M. Affronte, S. Carretta, P. Santini, G. Amoretti, R. S. G. Davies, G. Timco, and R. E. P. Winpenny, Phys. Rev. B **76**, 214405 (2007).
[8] J. Schnack and M. Luban, Phys. Rev. B **63**, 014418 (2000).
[9] O. Waldmann, T. Guidi, S. Carretta, C. Mondelli, and A. L. Dearden, Phys. Rev. Lett. **91**, 237202 (2003).
[10] O. Waldmann, Phys. Rev. B **65**, 024424 (2001).
[11] S. Carretta, J. van Slageren, T. Guidi, E. Liviotti, C. Mondelli, D. Rovai, A. Cornia, A. L. Dearden, F. Carsughi, M. Affronte, C. D. Frost, R. E. P. Winpenny, D. Gatteschi, G. Amoretti, and R. Caciuffo, Phys. Rev. B **67**, 094405 (2003).
[12] H. Yamazaki and K. Katsumata, Phys. Rev. B **54**, R6831 (1996).
[13] S. H. Glarum, S. Geschwind, K. M. Lee, M. L. Kaplan, and J. Michel, Phys. Rev. Lett. **67**, 1614 (1991).
[14] T. K. Ng, Phys. Rev. B **50**, 555 (1994).
[15] S. Qin, T. K. Ng, and Z. B. Su, Phys. Rev. B **52**, 12844 (1995).
[16] S. Miyashita and S. Yamamoto, Phys. Rev. B **48**, 913 (1993).
[17] S. Rakhmanova and D. L. Mills, Phys. Rev. B **54**, 9225 (1996).
[18] M. Sato and A. J. Sievers, Nature (London) **432**, 486 (2004).
[19] A. Franchini, V. Bortolani, and R. F. Wallis, Phys. Rev. B **73**, 054412 (2006).
[20] F. Troiani, A. Ghirri, M. Affronte, S. Carretta, P. Santini, G. Amoretti, S. Piligkos, G. Timco, and R. E. P. Winpenny, Phys. Rev. Lett. **94**, 207208 (2005).
[21] E. Micotti, Y. Furukawa, K. Kumagai, S. Carretta, A. Lascialfari, F. Borsa, G. A. Timco, and R. E. P. Winpenny, Phys. Rev. Lett. **97**, 267204 (2006).
[22] H. Wende, M. Bernien, J. Luo, C. Sorg, N. Ponpandian, J. Kurde, J. Miguel, M. Piantek, X. Xu, P. Eckhold, W. Kuch, K. Baberschke, P. M. Panchmatia, B. Sanyal, P. M. Oppeneer, and O. Eriksson, Nature Mater. **6**, 516 (2007).
[23] M. Mannini, P. Sainctavit, R. Sessoli, C. Cartier dit Moulin, F. Pineider, M.-A. Arrio, A. Cornia, and D. Gatteschi, Chem.-Eur. J. **14**, 7387 (2008).
[24] M. Mannini, F. Pineider, P. Sainctavit, C. Danieli, E. Otero, C. Sciancalepore, A. M. Talarico, M.-A. Arrio, A. Cornia, D. Gatteschi, and R. Sessoli, Nature Mater. **8**, 194 (2009).
[25] E. Dujardin, S. Ferlay, X. Phan, C. Desplanches, C. Cartier dit Moulin, P. Sainctavit, F. Baudelet, E. Dartyge, P. Veillet, and M. Verdaguer, J. Am. Chem. Soc. **120**, 11347 (1998).
[26] M.-A. Arrio, A. Scuiller, P. Sainctavit, C. Cartier dit Moulin, T. Mallah, and M. Verdaguer, J. Am. Chem. Soc. **121**, 6414 (1999).

[27] R. Moroni, Ch. Cartier dit Moulin, G. Champion, M.-A. Arrio, Ph. Sainctavit, M. Verdaguer, and D. Gatteschi, Phys. Rev. B **68**, 064407 (2003).
[28] V. Corradini, F. Moro, R. Biagi, U. del Pennino, V. De Renzi, S. Carretta, P. Santini, M. Affronte, J. C. Cezar, G. Timco, and R. E. P. Winpenny, Phys. Rev. B **77**, 014402 (2008).
[29] S. T. Ochsenbein, F. Tuna, M. Rancan, R. S. G. Davies, C. A. Muryn, O. Waldmann, R. Bircher, A. Sieber, G. Carver, H. Mutka, F. Fernandez-Alonso, A. Podlesnyak, L. P. Engelhardt, G. A. Timco, H. U. Güdel, and R. E. P. Winpenny, Chem.-Eur. J. **14**, 5144 (2008).
[30] E. C. Sanũdo, C. A. Muryn, M. A. Helliwell, G. A. Timco, W. Wernsdorfer, and R. E. P. Winpenny, Chem. Commun. (Cambridge) **2007**, 801.
[31] R. S. G. Davies, D. Collison, P. A. Mason, C. A. Muryn, E. C. Sanũdo, R. Sessoli, M. Shanmugam, G. A. Timco, F. Tuna, and R. E. P. Winpenny (unpublished).
[32] Crystallographic data (excluding structure factors) for the structures reported in this paper have been deposited with the Cambridge Crystallographic Data Centre as supplementary Publication Nos. CCDC 705752 and 705753. Copies of the data can be obtained free of charge on application to CCDC, 12 Union Road, Cambridge CB2 1EZ, UK, deposit@ccdc.cam.ac.uk.
[33] V. Bellini, A. Olivieri, and F. Manghi, Phys. Rev. B **73**, 184431 (2006).
[34] E. Liviotti, S. Carretta, and G. Amoretti, J. Chem. Phys. **117**, 3361 (2002).
[35] R. Caciuffo, T. Guidi, G. Amoretti, S. Carretta, E. Liviotti, P. Santini, C. Mondelli, G. Timco, C. A. Muryn, and R. E. P. Winpenny, Phys. Rev. B **71**, 174407 (2005).
[36] M. Evangelisti, F. Luis, L. J. de Jong, and M. Affronte, J. Mater. Chem. **16**, 2534 (2006).
[37] M. Affronte, J. C. Lasjaunias, and A. Cornia, Eur. Phys. J. B **15**, 633 (2000).
[38] Z. Salman, K. H. Chow, R. I. Miller, A. Morello, T. J. Parolin, M. D. Hossain, T. A. Keeler, C. D. P. Levy, W. A. MacFarlane, G. D. Morris, H. Saadaoui, D. Wang, R. Sessoli, G. G. Condorelli, and R. F. Kiefl, Nano Lett. **7**, 1551 (2007).
[39] L. Bogani, L. Cavigli, M. Gurioli, R. L. Novak, M. Mannini, A. Caneschi, F. Pineider, R. Sessoli, M. Clemente-León, E. Coronado, A. Cornia, and D. Gatteschi, Adv. Mater. **19**, 3906 (2007).
[40] S. Voss, M. Fonin, U. Rüdiger, M. Burgert, U. Groth, and Y. S. Dedkov, Phys. Rev. B **75**, 045102 (2007).
[41] V. Corradini, F. Moro, R. Biagi, V. De Renzi, U. del Pennino, V. Bellini, S. Carretta, P. Santini, V. A. Milway, G. Timco, R. E. P. Winpenny, and M. Affronte, Phys. Rev. B **79**, 144419 (2009).
[42] E. Gaudry, P. Sainctavit, F. Juillot, F. Bondioli, P. Ohresser, and I. Letard, Phys. Chem. Miner. **32**, 710 (2006).
[43] C. Theil, J. van Elp, and F. Folkmann, Phys. Rev. B **59**, 7931 (1999).
[44] B. T. Thole, G. van der Laan, J. C. Fuggle, G. A. Sawatzky, R. C. Karnatak, and J.-M. Esteva, Phys. Rev. B **32**, 5107 (1985); B. T. Thole, G. van der Laan, and P. H. Butler, Chem. Phys. Lett. **149**, 295 (1988).
[45] F. M. F. de Groot, J. Electron Spectrosc. Relat. Phenom. **67**, 529 (1994); Chem. Rev. (Washington, D.C.) **101**, 1779 (2001).
[46] J. van Elp and B. G. Searle, J. Electron Spectrosc. Relat. Phenom. **86**, 93 (1997).
[47] G. Champion, N. Lalioti, V. Tangoulis, M.-A. Arrio, P. Sainctavit, F. Villain, A. Caneschi, D. Gatteschi, C. Giorgetti, F. Baudelet, M. Verdaguer, and C. Cartier dit Moulin, J. Am. Chem. Soc. **125**, 8371 (2003).
[48] P. Carra, B. T. Thole, M. Altarelli, and X. Wang, Phys. Rev. Lett. **70**, 694 (1993).
[49] B. T. Thole, P. Carra, F. Sette, and G. van der Laan, Phys. Rev. Lett. **68**, 1943 (1992).
[50] P. Sainctavit, J. Electron Spectrosc. Relat. Phenom. **86**, 133 (1997).
[51] J. P. Crocombette, B. T. Thole, and F. Jollet, J. Phys.: Condens. Matter **8**, 4095 (1996).
[52] J. Stohr, J. Magn. Magn. Mater. **200**, 470 (1999).
[53] C. T. Chen, Y. U. Idzerda, H. J. Lin, N. V. Smith, G. Meigs, E. Chaban, G. H. Ho, E. Pellegrin, and F. Sette, Phys. Rev. Lett. **75**, 152 (1995).
[54] Y. Teramura, A. Tanaka, and T. Jo, J. Phys. Soc. Jpn. **65**, 1053 (1996).
[55] E. Goering, Philos. Mag. **85**, 2895 (2005), and references therein.